Heliyon 10 (2024) e38144

Contents lists available at ScienceDirect

Heliyon

journal homepage: www.cell.com/heliyon

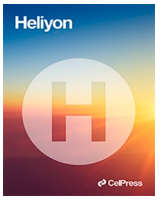

Research article

Enhanced phosphorus adsorption using modified drinking water treatment residues: A comparative analysis of powder and alginate bead forms

Sitthichai Chaikhan, Somjate Thongdamrongtham *, Supanee Junsiri, Chiraporn Labcom, Anootsara Sarak, Laksanee Boonkhao

College of Medicine and Public Health, Ubon Ratchathani University, Ubon Ratchathani, Thailand

ARTICLE INFO

Keywords:
Phosphorus adsorption
Modified drinking water treatment residues (MDWTR)
Adsorption kinetics
Adsorption isotherms
Toxicity characteristic leaching procedure (TCLP)
In vitro bioaccessibility (IVBA)
Wastewater treatment

ABSTRACT

This study provides an analysis of the phosphorus adsorption efficacy of three modified drinking water treatment residues (MDWTRs): MDWTR-P (powdered form), MDWTR-D2, and MDWTR-D5 (alginate bead-entrapped forms with bead diameters of 2 mm and 5 mm, respectively). The preparation process involved washing and drying the drinking water treatment residue, followed by grinding and sieving to achieve particle sizes below 90 μm. The residue was then incinerated at 600 °C in oxygen-limited conditions. Subsequently, the MDWTR was formulated into alginate beads by mixing with sodium alginate and $FeCl_3$ solutions, resulting in spherical particles of specified diameters. The evaluation of surface area, pore volume, pore size, and CHN concentration revealed that MDWTR-D5 possesses the largest surface area (284.7 $m^2\ g^{-1}$) and highest micropore volume (0.04 $cm^3\ g^{-1}$), indicating a greater capacity for adsorption. SEM-EDS analysis demonstrated significant compositional changes post-treatment, particularly elevated phosphorus levels, confirming effective adsorption. Metal content analysis indicated high aluminum levels in MDWTR-P and increased iron content in MDWTR-D5. Toxicity Characteristic Leaching Procedure (TCLP) and *in vitro* bioaccessibility (IVBA) tests confirmed the non-hazardous nature of all MDWTRs, ensuring their safety for environmental applications. Kinetic analyses using pseudo-first-order, pseudo-second-order, and intraparticle diffusion models highlighted the superior performance of MDWTR-D5, with the highest equilibrium adsorption capacity and initial adsorption rate across all tested concentrations, suggesting both high efficiency and rapid adsorption potential. Further validation using Langmuir and Freundlich isotherms revealed MDWTR-D5's highest monolayer adsorption capacity (22.88 mg g^{-1}) and Freundlich adsorption capacity parameter (6.97 mg g^{-1}). Statistical analysis via one-way ANOVA confirmed significant differences in phosphorus concentrations among the MDWTRs samples (p-value <0.001), consistently underscoring MDWTR-D5's superior adsorption performance. These findings highlight MDWTR-D5's potential as an effective adsorbent for phosphorus removal in wastewater treatment, emphasizing its applicability in environmental remediation strategies.

* Corresponding author.
E-mail address: Somjate.t@ubu.ac.th (S. Thongdamrongtham).

https://doi.org/10.1016/j.heliyon.2024.e38144
Received 7 July 2024; Received in revised form 6 September 2024; Accepted 18 September 2024
Available online 25 September 2024

1. Introduction

The presence of phosphorus contamination in water bodies is a significant environmental issue worldwide, which has extensive implications for the health of ecosystems, the quality of water, and the well-being of humans [1,2]. Phosphorus pollution in Thailand is a multifaceted issue, primarily driven by activities in the fisheries, livestock, and agricultural sectors, as well as urban waste management [3,4]. Elevated phosphorus concentrations can result in eutrophication, a process characterized by detrimental algal blooms, depletion of oxygen, and a reduction in biodiversity, ultimately undermining the ecological balance of aquatic environments [5,6]. The reported total phosphorus (TP) concentration in Bangkok's domestic wastewater, ranging from 0.6 to 1.05 mg L^{-1}, indeed presents a significant concern for water quality management, as this level of phosphorus can contribute to eutrophication in receiving water bodies if not adequately treated before discharge [7]. In addition, eutrophication has substantial economic implications, affecting sectors such as agriculture, fishing, and tourism, and jeopardizing the long-term viability of water resources [8,9]. Efficient phosphorus removal is crucial in wastewater treatment to reduce the negative impacts of phosphorus contamination and to meet the legal requirements for releasing treated wastewater [10]. Conventional techniques, such as coagulation precipitation, have been extensively utilized in wastewater treatment facilities to eliminate phosphorus [11,12]. Nevertheless, these approaches have several disadvantages, such as exorbitant operational expenses, production of substantial quantities of sludge, and potential environmental hazards linked to sludge disposal [13]. However, the adsorption process offers a promising alternative, as it has been well described by Langmuir and Freundlich isotherms, with regression coefficients (R^2 and Adj. R^2) close to 1, confirming the model's fitness [14].

Recently, there has been increasing interest in investigating alternative methods for removing phosphorus via wastewater treatment, with an emphasis on ecological and economical alternatives. Among these options, drinking water treatment residuals (DWTRs) have emerged as potential choices for absorbing phosphorus [15]. DWTRs are the residual substances that are formed as a result of treating untreated water to make it safe for drinking [16]. These residues primarily contain inorganic substances like aluminum and iron hydroxides, along with organic matter [17]. Due to their natural ability to adsorb substances, DWTRs are highly desirable for removing phosphorus in wastewater treatment [18,19]. Additionally, their availability as byproducts of drinking water treatment procedures further enhances their appeal. Furthermore, DWTRs can be altered using diverse methods to augment their ability to absorb phosphorus, providing possibilities to raise the efficiency and efficacy of phosphorus elimination in wastewater treatment facilities. Investigations into the alteration of DWTRs have produced encouraging outcomes, since studies have shown the effectiveness of modified DWTRs in eliminating phosphorus from wastewater [20,21]. Studies have demonstrated that employing methods like oxygen-limited heat treatment can improve the ability of DWTRs to absorb phosphorus by modifying their physical and chemical characteristics, such as surface area and porosity [22–24]. The integration of DWTRs into treatment media, such as bioretention systems, has been shown to enhance phosphorus removal efficiency in comparison to systems that do not include DWTRs [25–27]. In addition, novel methods, such as enclosing granular DWTRs in alginate beads, have been created to tackle the difficulties related to the management and use of DWTRs in wastewater treatment procedures [27]. Alginate beads containing granular DWTRs have benefits such as enhanced mechanical stability, higher surface area, and improved phosphorus adsorption capability [28]. These characteristics make them suitable for practical use in wastewater treatment systems. Applying the Langmuir isotherm and Freundlich model to analyze the adsorption process of MDWTRs provides valuable understanding of the phosphorus removal mechanism [29]. The Langmuir isotherm postulates the adsorption of a single layer on a uniform surface, whereas the Freundlich model characterizes the adsorption of many layers on non-uniform surfaces [25,30]. The suitability of these models indicates that the process of phosphorus adsorption onto MDWTRs primarily happens as a single layer on a uniform surface, emphasizing the potential of MDWTRs as an effective adsorbent for eliminating phosphorus in wastewater treatment applications [31–33] In parallel with these developments, recent studies have enhanced adsorbents using techniques such as Central Composite Design (CCD) with Multi-Walled Carbon Nanotubes (MCSMWCNTs), achieving an adsorption capacity of 256.4 mg g^{-1} for Acetaminophen (ACT). The Langmuir and pseudo-second-order kinetic models showed the best performance in these studies, highlighting the efficiency of MCSMWCNTs in removing ACT from aqueous solutions [34]. Additionally, Carbon Quantum Dots (CQDs) have garnered attention for their versatility, cost-effectiveness, and ease of synthesis, making them promising candidates for water and wastewater treatment applications [35]. Furthermore, Mg-Al-LDH-based adsorbents have demonstrated a high removal efficiency of diethyl phthalate (DEP), achieving a removal efficiency of 96.7 % and an adsorption capacity of 101.6 mg g^{-1} [36]. These advancements collectively demonstrate the increasing potential of innovative adsorbents in improving the effectiveness of water treatment processes.

This study aims to rigorously compare the phosphorus adsorption efficiency of three distinct forms of modified drinking water treatment residues (MDWTRs), each with particle sizes below 90 μm, which have been subjected to incineration at 600 °C in an oxygen-limited environment. The MDWTRs were prepared in both powdered form and as alginate beads with diameters of 2 mm and 5 mm. Comprehensive physical and chemical characterization was performed using advanced analytical techniques such as BET for surface area and porosity analysis, FTIR for functional group identification, XRF for elemental composition, SEM-EDS for surface morphology and elemental distribution, and ICP-OES for metal content analysis.

The study also examined phosphorus adsorption kinetics and isotherms, employing models such as the Langmuir and Freundlich isotherms to elucidate the adsorption mechanisms. The influence of pH on adsorption was systematically investigated across a range of conditions to determine optimal operational parameters. Additionally, the environmental safety of the MDWTRs was assessed through the Toxicity Characteristic Leaching Procedure (TCLP) and *in vitro* bioaccessibility (IVBA) tests, ensuring the non-hazardous nature of the materials and their suitability for environmental applications.

2. Material and methods

2.1. Material

The following chemicals were used in the study: sodium alginate ($NaC_6H_7O_6$) was obtained from Sisco Research Laboratories Pvt. Ltd., India. Ferric chloride ($FeCl_3$) was sourced from Loba Chemie Pvt. Ltd., India. Acetic acid-sodium acetate was provided by Inter Education Supply Co., Ltd., Thailand. Laboratory-grade hydrochloric acid (HCl) was also utilized. Potassium dihydrogen phosphate (KH_2PO_4) was acquired from Ajax Finechem, Thermo Fisher Scientific, Australia. All chemicals were of analytical grade, and deionized water was used for preparing solutions.

2.2. Preparation of MDWTRs

The DWTR collected from the Ubon Ratchathani water supply point underwent a series of preparation steps for analysis. Initially, the samples were washed thrice with deionized water, followed by drying at 103–105 °C for 24 h. Subsequently, they were ground and sieved through 180 mesh to obtain particle sizes <90 μm. The resulting samples were then subjected to incineration in an oxygen-limited muffle furnace at 600 °C for 10 h (ISOLAB Laborgeräte GmbH, Germany), followed by cooling in a desiccator for 1 h (S.P. Dry Module, Japan), resulting in what is termed as modified drinking water treatment residue (MDWTRs). This modified residue is stored in moisture-free containers and referred to as MDWTR-P when in powder form [37].

2.3. Preparation of granular MDWTRs

Create a sodium alginate solution with a concentration of 2 % (w/v) by dissolving sodium alginate ($NaC_6H_7O_6$) in 100 ml of deionized water. Continuously agitate the solution until it has a uniform and consistent composition. Subsequently, include 50 g of the previously made MDWTRs into the solution, gradually and while stirring, in order to achieve a uniform and consistent combination. Next, create a solution by dissolving 2 % (w/v) $FeCl_3$ in deionized water, with a volume of 100 ml. Next, employ a pipette to take out the MDWTRs and dispense them into the $FeCl_3$ solution, resulting in the formation of particles with a spherical morphology [28,38]. The volume of MDWTRs is subsequently modified to achieve diameters of 2 mm (MDWTR-D2) and 5 mm (MDWTR-D5). Subsequently, the material is immersed for a duration of 4 h, followed by three rinses with deionized water. It is then subjected to a drying process at a temperature of 60 °C for 2 h, before being positioned. Allow to cool at ambient temperature. Place the substance in a beaker and cover it with foil. Then, store it in a desiccant cabinet to be used in the subsequent experiment.

2.4. The lability of heavy metals

2.4.1. The toxicity characteristic leaching procedure (TCLP)

Prepare a 20 mL solution of acetic acid-sodium acetate and adjust the pH to 4.93 ± 0.05. Add 1 g of each of the three varieties of MDWTRs to the solution and stir at a speed of 150 rpm for 18 h. After the stirring period, filter the sample using 0.45 μm cellulose acetate filter paper. Subsequently, transfer 10 mL of the filtered sample into a test tube and ensure it is securely sealed. Conduct heavy metal analysis using Inductively Coupled Plasma Optical Emission Spectrometry (ICP-OES), specifically with the Optima 8000 ICP-OES (PerkinElmer, Inc., Waltham, USA). The analysis will include the detection of arsenic, lead, cobalt, cadmium, mercury, iron, manganese, calcium, and aluminum.

2.4.2. The process of in vitro bioaccessibility (IVBA)

To prepare a 0.4 M glycine solution with a final volume of 100 mL, dissolve the appropriate amount of glycine in distilled water. Adjust the pH of the solution to 1.5 ± 0.5 at 37 °C using laboratory-grade hydrochloric acid (HCl). Subsequently, supplement each type of MDWTR into three separate experimental sets, with each set containing 1 g. Place the samples in a shaking incubator set at 30 rpm and 37 °C for 1 h. After the incubation period, ensure that the pH value remains within ±0.5 of the initial pH. Next, filter the samples through a 0.45 μm cellulose acetate filter. Measure and record the volume of the filtrate, ensuring it is 10 mL. Submit the filtered samples for analysis to determine the concentration of heavy metals, following the procedure outlined in Experiment 2.3.1. Calculate the *in vitro* bioaccessibility (IVBA) using the following formula (1):

$$\textit{In vitro bioaccessibility } (IVBA) = \frac{HM_{ext} \cdot V_{ext} \cdot 100}{HM_{MDWTR} \cdot MDWTR_{mass}} \quad (1)$$

where: HM = heavy metal, HM_{ext} = *in vitro* extractable heavy metal in the *vitro* extract (mg L^{-1}), V_{ext} = volume of extraction solution (L), HM_{MDWTR} = heavy metal concentration in the MDWTRs sample (mg kg^{-1}), and $MDWTR_{mass}$ = mass of MDWTRs sample (kg) [39]

2.5. Effect of pH on phosphorus adsorption

Prepare potassium dihydrogen phosphate (KH_2PO_4) solutions with phosphorus concentrations of 50, 100, and 500 mg L^{-1}. Aspirate 50 mL of each solution and adjust their pH levels to 3, 5, 7, 9, and 11, respectively. Add 0.5 g of each type of MDWTRs to separate Erlenmeyer flasks containing the solutions, ensuring triplicate testing for each concentration and pH condition. Shake the mixtures at

100 rpm for 48 h to reach equilibrium. After equilibration, measure the phosphorus content in the samples using the ascorbic acid method [40].

2.6. The characterization of powder and granular MDWTRs

For the characterization of MDWTRs (MDWTR-P, MDWTR-D2, and MDWTR-D5), several analyses were performed. Specific surface area (SSA) analysis, pore volume determination, and gas adsorption measurements were conducted using the BET method on a 5-g sample with the QUADRASORB evo Gas Sorption Surface Area and Pore Size Analyzer (Anton Paar, Graz, Austria). Surface morphology was examined via scanning electron microscopy (SEM) and energy-dispersive X-ray spectroscopy (SEM-EDS) on a 10-g sample, utilizing the JEOL JSM-6010 LA, JSM-7610F Plus (Tokyo, Japan). Additionally, metal content analysis, including arsenic, lead, cobalt, cadmium, mercury, iron, manganese, calcium, and aluminum, was performed using inductively coupled plasma optical emission spectrometry (ICP-OES) with the Optima 8000 ICP-OES (PerkinElmer, Inc., Waltham, USA) on a 10-g sample. For elemental composition analysis, X-ray fluorescence (XRF) was conducted using the Rigaku ZSX Primus (Tokyo, Japan) on a 10-g sample. Fourier-transform infrared spectroscopy (FT-IR) was carried out on a 5-g sample with the Nicolet 6700 FT-IR Spectrometer (Thermo Fisher Scientific, Waltham, USA). The carbon, hydrogen, and nitrogen content was assessed using the LECO CHN628 analyzer (Saint Joseph, USA) on a 5-g sample.

2.7. Adsorption kinetics

Prepare solutions of KH_2PO_4 with phosphorus concentrations of 0, 50, 100, 250, and 500 mg L^{-1}, maintaining a pH range of 6–6.5. Transfer 100 mL of each solution into separate 100 mL Erlenmeyer flasks. Add 1 g of MDWTRs in powder form, D2, and D5 to separate flasks, creating distinct experimental batches for each type of MDWTR. Conduct duplicate experiments by shaking the mixtures at 100 rpm and maintaining a temperature of 25 °C. At specified intervals of 2, 4, 6, 8, 10, 12, 24, 48, and 72 h, take 10 mL samples to measure soluble reactive phosphorus (SRP) using the ascorbic acid method [40].

To gain deeper insights into the adsorption kinetics, the experimental data were analyzed by employing the pseudo-first-order kinetic model (Eq. (2)) and the pseudo-second-order kinetic model (Eq. (3)), which are widely utilized for elucidating the rate-determining step and the potential mechanism governing the adsorption process [41].

$$q_t = q_e\left(1 - e^{-k_1 t}\right) \tag{2}$$

$$\frac{t}{q_t} = \frac{1}{k_2 \cdot q_e^2} + \frac{t}{q_e} \tag{3}$$

In these equations, q_t and q_e represent the amounts of P adsorbed onto the granular DWTR (mg g^{-1}) at time t and at equilibrium, respectively. k_1 denotes the rate constant associated with the pseudo-first-order kinetic model (h^{-1}), while k_2 is the rate constant corresponding to the pseudo-second-order kinetic model (g mg^{-1} h^{-1}).

To investigate whether intraparticle diffusion governs the rate-determining step in the adsorption process, the adsorption kinetic data were analyzed using the intraparticle diffusion model, also known as the Weber-Morris equation, represented by Ref. [42] by Eq. (4):

$$qt = kid \times t^{1/2} + C \tag{4}$$

where qt denotes the amount of adsorbate (phosphorus) adsorbed at time t (mg g^{-1}), kid is the intraparticle diffusion rate constant (mg $g^{-1}\cdot min^{-1/2}$), kid can be evaluated from the slope of the linear plot of qt versus $t^{1/2}$, the intercept of which reflects the boundary layer effect [42]. Then t represents the time (min), and C is the intercept related to the boundary layer thickness (mg g^{-1}).

2.8. Adsorption isotherm

Prepare solutions of KH_2PO_4 with phosphorus concentrations of 0, 0.2, 2, 10, 20, 100, and 200 mg L^{-1}. Transfer 100 mL of each solution into separate 100 mL Erlenmeyer flasks. Add 1 g of MDWTRs in powder form, D2, and D5 to separate flasks, creating distinct experimental batches for each type of MDWTRs. Conduct triplicate experiments by shaking the flasks at 100 rpm at a temperature of 25 °C. After 48 h, which corresponds to the equilibrium time determined in adsorption kinetics tests, collect 10 mL samples in order to quantify soluble reactive phosphorus (SRP) using the ascorbic acid method. A sample of 3 g of each type of MDWTR, initially containing 200 mg of phosphorus, was subjected to comprehensive analytical techniques including Scanning Electron Microscopy (SEM), Energy Dispersive X-ray Spectroscopy (SEM-EDS), Fourier Transform Infrared Spectroscopy (FTIR), and X-ray Fluorescence (XRF) analysis.

The Langmuir isotherm equation is expressed by Eq. (5) [28]:

$$q_e = \frac{q_m \cdot K_L . C_e}{1 + K_L \cdot C_e} \tag{5}$$

where q_e is the amount of adsorbed P at equilibrium (mg g^{-1}), C_e is the P concentration of the supernatant at equilibrium (mg L^{-1}), q_m

represents the maximum monolayer adsorption capacity (mg g^{-1}), and K_L is the constant of the Langmuir isotherm relevant to adsorption energy.

A separation factor, commonly used to characterize the Langmuir isotherm, is defined by Eq. (6):

$$R_L = \frac{1}{1 + K_L \cdot C_0} \tag{6}$$

where C_0 is the initial P concentration (mg L^{-1}).

The Freundlich isotherm is an empirical model that accounts for multilayer adsorption on heterogeneous surfaces. The corresponding mathematical expression is represented by Eq. (7) [28]:

$$q_e = K_F \cdot C_e^{1/n} \tag{7}$$

where q_e is the amount of P adsorbed at equilibrium (mg g^{-1}), C_e is the P concentration in the supernatant at equilibrium (mg L^{-1}), and K_F and $1/n$ are the Freundlich constants, representing the adsorption capacity and intensity, respectively.

To evaluate the statistical significance of the adsorption performance among the three forms of MDWTRs, a one way analysis of variance (ANOVA) was conducted on the experimental data.

3. Results

3.1. The characterization of powder and granular MDWTRs

3.1.1. Surface area, pore volume, pore size and CHN content

The surface area, pore volume, pore size, and CHN content characteristics of three materials, MDWTR-P, MDWTR-D2, and MDWTR-D5, were examined. Surface area measurements, performed using several methods such as single point BET, multi point BET, Langmuir surface area, and BJH cumulative adsorption, consistently showed that MDWTR-D5 had the largest surface area compared to the other two. The surface area measurements for MDWTR-D5 varied from 39.53 $m^2 g^{-1}$ (determined using the BJH method) to 284.7 $m^2 g^{-1}$ (determined using the Langmuir surface area method). MDWTR-D2 had the highest overall pore volume (0.2119 $cm^3 g^{-1}$) and BJH cumulative adsorption pore volume (0.1934 $cm^3 g^{-1}$) among the samples. On the other hand, MDWTR-D5 had the greatest micropore volume according to the HK technique, measuring 0.0448 $cm^3 g^{-1}$. MDWTR-P had the greatest average pore radius (57.2 Å) among the samples, when considering pore size. Nevertheless, all three materials exhibited comparable BJH adsorption pore radii, measuring roughly 17.99 Å, as well as HK method pore radii of 1.838 Å. The carbon content was higher in MDWTR-D2 and MDWTR-D5 than in MDWTR-P, likely due to chemical modifications. Hydrogen content remained consistent across all materials, while nitrogen content showed minor variations, with MDWTR-D2 and MDWTR-D5 slightly higher than MDWTR-P. For many applications involving adsorption, it is crucial to have a large surface area, a significant volume of pores, and a suitable distribution of pore sizes. Detailed results are presented in Table 1.

Table 1
Comparative analysis of surface area, pore volume, pore size, and carbon, hydrogen, and nitrogen content in MDWTR-P, MDWTR-D2, and MDWTR-D5 materials.

Specific Surface Area	MDWTR-P	MDWTR-D2	MDWTR-D5
Single point BET ($m^2 g^{-1}$)	68.76	75.45	107.3
Multi point BET ($m^2 g^{-1}$)	69.89	79.53	109.2
Langmuir surface area ($m^2 g^{-1}$)	245.3	262.2	284.7
BJH method ($m^2 g^{-1}$)	46.57	49.47	39.53
Pore Volume			
Total pore volume for pores with radius ($cm^3 g^{-1}$)	0.1999	0.2119	0.1663
BJH method ($cm^3 g^{-1}$)	0.1907	0.1934	0.1257
HK method microscope volume ($cm^3 g^{-1}$)	0.02835	0.02956	0.0448
Pore Size			
Average pore radius (Å)	57.2	53.28	30.44
BJH method adsorption pore radius (Å)	17.99	17.99	17.98
HK method pore radius (Å)	1.838	1.838	1.838
CHN content			
Carbon, C (%)	0.90 ± 0.004	0.96 ± 0.057	0.94 ± 0.065
Hydrogen, H (%)	1.24 ± 0.360	1.01 ± 0.060	1.09 ± 0.050
Nitrogen, N (%)	0.06 ± 0.002	0.08 ± 0.004	0.08 ± 0.005

Remark: BJH (Barrett-Joyner-Halenda), HK (Horvath-Kawazoe) BJH is typically used for mesopores (2–50 nm), while HK is used for micropores (<2 nm).

3.1.2. The FTIR spectra

The MDWTR-P, MDWTR-D2, and MDWTR-D5 samples were analyzed using Fourier Transform Infrared (FTIR) spectroscopy. Fig. 1 displays the results of the analysis. These results offer vital information about the chemical compositions and molecular structures of the samples. The spectra of MDWTR-P before adsorption have a wide frequency range of 3000–3500 cm^{-1}, indicating the presence of stretching vibrations of O-H bonds. This suggests the existence of hydroxyl groups or water molecules. Furthermore, the existence of silicate or silica-based substances can be deduced from the peak detected at around 1022 cm^{-1}. Moreover, the complex peaks observed in the fingerprint region (500–1500 cm^{-1}) indicate a wide range of bending vibrations of functional groups. Following the process of adsorption, a decrease in the frequency range indicates a decrease in hydroxyl groups or water molecules, while the emergence of a new peak at around 1630 cm^{-1} indicates the existence of carbonyl compounds or other functional groups containing carbon-oxygen bonds. Similarly, in the case of MDWTR-D2, there are notable absorption bands ranging from 407.41 to 3372.41 cm^{-1} before adsorption. Bands below 1000 cm^{-1} may suggest the presence of bending and stretching vibrations of alkyl groups or aromatic rings. The band observed at 1610.71 cm^{-1} suggests the presence of carbonyl (C=O) groups or aromatic ring vibrations. On the other hand, the broad band observed at 3372.41 cm^{-1} shows the existence of hydroxyl (O-H) or amine (N-H) groups. After the adsorption process, there are observed absorption bands spanning from 474.12 to 3278.52 cm^{-1}. These bands have comparable meanings in terms of the functional groups present. Moreover, the FTIR spectra of MDWTR-D5, both prior to and following adsorption, exhibit bands primarily within the 400–3400 cm^{-1} range. The lower wavenumber bands suggest vibrations related to the bending and stretching of alkyl groups or aromatic rings, while the higher wavenumber bands indicate the presence of carbonyl (C=O) groups or hydroxyl (O-H) and amine (N-H) groups.

3.1.3. Adsorption characteristics and the relationship between pore volume and pore diameter

The diagram (Fig. 2) depicts the comprehensive adsorption properties of three different materials: MDWTR-P, MDWTR-D2, and MDWTR-D5. The observed correlation between an increase in relative pressure and a rise in adsorption across all materials provides strong evidence for the existence and reliability of the adsorption process within the analyzed systems. Nevertheless, the noticeable changes in the contours of the lines and the ability of the materials to adsorb at various relative pressures indicate subtle disparities in their adsorption characteristics and capabilities, hence strengthening the reliability and strength of our results. Furthermore, a comprehensive examination of the correlation between pore volume (expressed in $cm^3\ g^{-1}$) and pore diameter (measured in Å) was provided for the three substances. MDWTR-P has a distinctively limited range of pore diameters, with the majority of the volume centered within a pore diameter of 20–25 Å. On the other hand, MDWTR-D2 exhibits a wider range of pore sizes, with a notable amount of small pores and a smaller proportion of medium-sized pores. Among the options, MDWTR-D5 has the highest overall pore volume, with MDWTR-D2 and MDWTR-P following closely behind. The information about the distribution of pore sizes emphasizes the dependability and importance of these discoveries. It also highlights the possible uses of these materials in different adsorption processes, where micropores and mesopores have separate but crucial functions based on their accessibility and dimensions.

3.1.4. Characterization of MDWTRs samples using SEM and SEM-EDS analysis

Based on the comprehensive SEM-EDS analysis of MDWTR-P, MDWTR-D2, and MDWTR-D5 samples, significant compositional changes were observed before and after the adsorption process. MDWTR-P, initially composed primarily of silicon (47.60 %), aluminum (30.50 %), and iron (14.10 %), exhibited a remarkable 432.69 % increase in phosphorus content (from 0.52 % to 2.77 %) post-treatment. MDWTR-D2 showed more pronounced alterations, with notable decreases in silicon (−10.69 %) and aluminum (−9.12 %), coupled with an 11.62 % increase in iron content and a striking 1042.86 % increase in phosphorus (from 0.49 % to 5.60 %). MDWTR-D5 displayed a unique pattern with a slight increase in silicon (5.08 %), stable aluminum levels, a decrease in iron (−5.67 %), and a substantial 776.09 % increase in phosphorus (from 0.46 % to 4.03 %). Across all samples, a consistent increase was observed for phosphorus. High-resolution SEM micrographs corroborated the EDS findings, revealing substantial modifications in surface

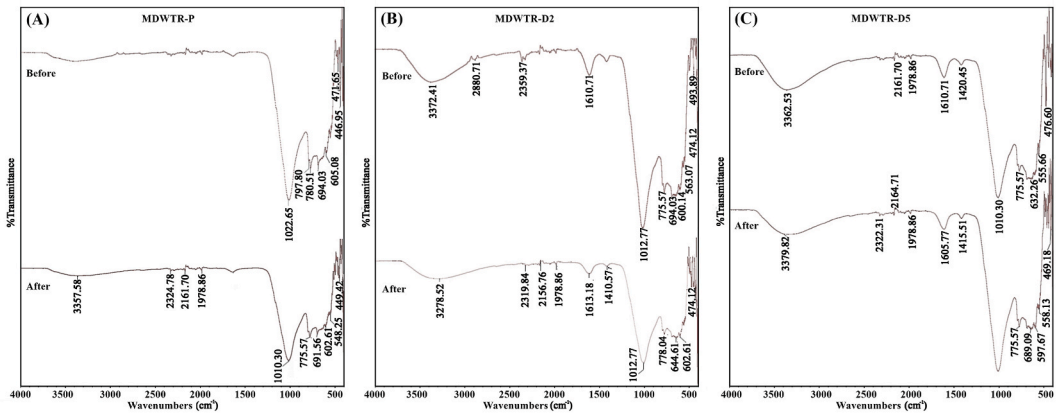

Fig. 1. The FTIR spectra for three different materials labeled as (A) MDWTR-P, (B) MDWTR-D2, and (C) MDWTR-D5 before and after the adsorption experiment.

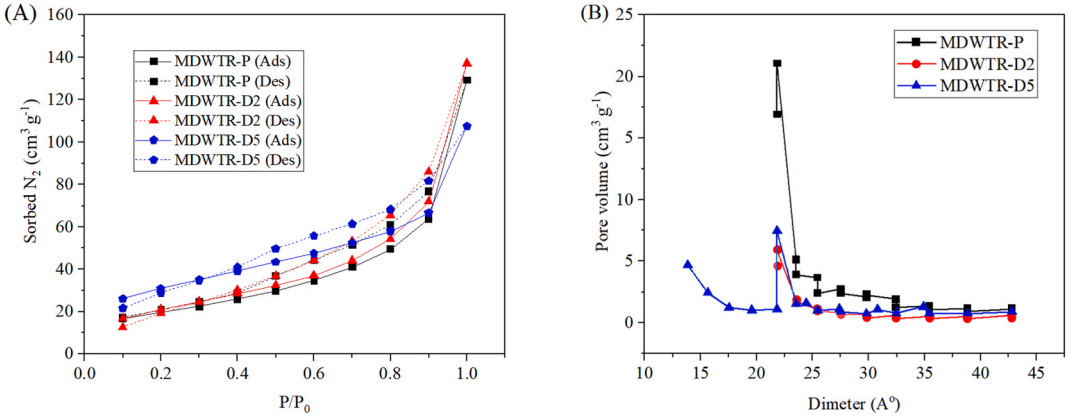

Fig. 2. (A) Depicts the nitrogen adsorption and desorption isotherms, while (B) illustrates the pore size distributions for the materials MDWTR-P, MDWTR-D2, and MDWTR-D5.

morphology and texture across all MDWTR materials post-treatment. The observed physical alterations, characterized by increased surface roughness and expanded surface area, are hypothesized to significantly enhance adsorption efficacy by creating additional active sites for phosphorus binding. Detailed results, including high-resolution micrographs and elemental distribution, are presented in Fig. 3 and Table 2.

3.2. The lability of heavy metals

The TMC analysis identified substantial disparities in the concentrations of several components among the samples. Significantly, MDWTR-P had the greatest Total Metal Concentration (TMC) for aluminum (170,165.68 mg kg^{-}), whereas MDWTR-D5 exhibited the highest TMC for iron (87,519.07 mg kg^{-}). MDWTR-D5 had the highest TMC for calcium (4986.31 mg kg^{-1}) and manganese (1163.82

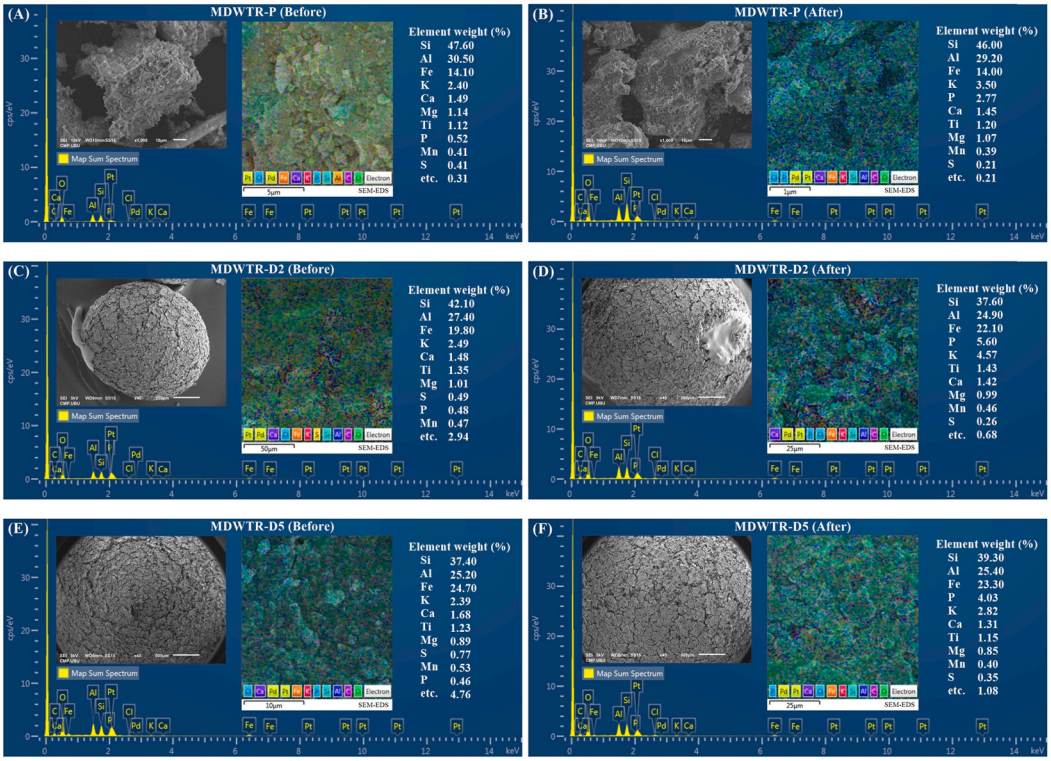

Fig. 3. SEM-EDS mapping illustrating phosphorus and elemental distribution before and after adsorption on (A–B) MDWTR-P, (C–D) MDWTR-D2, and (E–F) MDWTR-D5.

Table 2
Elemental distribution before and after adsorption on three different materials: MDWTR-P, MDWTR-D2, and MDWTR-D5.

Element	MDWTR-P			MDWTR-D2			MDWTR-D5		
	Before	After	%Change	Before	After	%Change	Before	After	%Change
Si	47.60	46.00	−3.36	42.10	37.60	−10.69	37.40	39.30	5.08
Al	30.50	29.20	−4.26	27.40	24.90	−9.12	25.20	25.40	0.79
Fe	14.10	14.00	−0.71	19.80	22.10	11.62	24.70	23.30	−5.67
K	2.40	2.5	4.17	2.40	4.57	90.42	2.39	2.82	17.99
Ca	2.10	1.45	−30.95	1.48	1.43	−3.38	1.68	1.31	−22.02
Ti	1.12	1.20	7.14	1.35	1.43	5.93	1.23	1.15	−6.50
Mg	1.14	1.07	−6.14	1.01	0.99	−1.98	0.89	0.85	−4.49
P	0.52	2.77	432.69	0.49	5.60	1042.86	0.46	4.03	776.09
Mn	0.41	0.39	−4.88	0.47	0.46	−2.13	0.53	0.40	−24.53
S	0.41	0.21	−48.78	0.49	0.26	−46.94	0.77	0.35	−54.55
etc.	0.31	0.21	−32.26	2.94	0.68	−76.87	4.76	1.08	−77.31

mg kg^{-}). The presence of Co, As, Cd, Hg, and Pb was not observed in MDWTR-D2 and MDWTR-D5. However, MDWTR-P did contain a minor quantity of Co (3.70 mg kg^{-}). The TCLP results revealed that MDWTR-P had the highest concentration of leachable aluminum (1383.00 mg L^{-1}), as well as the highest quantities of leachable iron (65.33 mg L^{-1}) and calcium (72.43 mg L^{-1}). The TCLP values for Mn were rather low and similar among the three samples. The IVBA analysis, which assesses the bioaccessibility of elements, found that MDWTR-P had the greatest IVBA percentages for Al (7.48 %), Fe (4.40 %), Ca (33.56 %), and Mn (17.27 %). MDWTR-D2 and MDWTR-D5 displayed decreased IVBA values for these elements, indicating a diminished bioaccessibility in comparison to MDWTR-P. These findings emphasize the differences in the metal concentration, leachability, and bioaccessibility among the samples of municipal drinking water, which could affect their potential environmental impact and appropriateness for various uses. Detailed results are presented in Table 3.

3.3. *Effect of pH on phosphorus adsorption*

The phosphorus (P) removal effectiveness of the MDWTR samples, namely MDWTR-P, MDWTR-D2, and MDWTR-D5, was thoroughly assessed across different pH levels and baseline P concentrations. The results showed consistent and highly effective performance of the MDWTR samples under diverse situations. The MDWTR-P consistently produced P removal rates of above 98 % at all pH levels. The highest removal efficiency, reaching around 99.9 %, was seen within the pH range of 3–9 for all starting concentrations. Similarly, MDWTR-D2 consistently achieved removal efficiencies of over 98 %, with the maximum efficiency of almost 99.9 % reported at pH levels of 5 and 7 for all concentrations. Meanwhile, MDWTR-D5 had significantly lower removal rates than MDWTR-P and MDWTR-D2; it nevertheless had a removal rate of over 98 % in most cases. Its highest effectiveness was observed at pH levels of 3 and 7. The extensive findings highlight the outstanding and consistent efficiency of MDWTR materials in removing phosphorus from solutions, especially at pH levels of approximately 5 and 7, regardless of the initial concentration of phosphorus. Detailed results are presented in Fig. 4.

Table 3
Evaluated total metal content (TMC), leachability (TCLP), and *in vitro* bioaccessibility (IVBA) of various elements present in the MDWTR-P, MDWTR-D2, and MDWTR-D5 samples.

Element	Sample	TMC(mg kg^{-1})	TCLP(mg L^{-1})	IVBA(%)
Al	MDWTR-P	170,165.68	1383.00	7.48
	MDWTR-D2	152,870.15	446.8	5.12
	MDWTR-D5	140,595.91	439.55	6.02
Fe	MDWTR-P	15,082.98	65.33	4.40
	MDWTR-D2	70,156.99	47.72	1.79
	MDWTR-D5	87,519.07	46.39	1.24
Ca	MDWTR-P	1147.28	72.43	33.56
	MDWTR-D2	4392.70	39.66	22.31
	MDWTR-D5	4986.31	53.69	18.45
Mn	MDWTR-P	287.36	6.54	17.27
	MDWTR-D2	1029.87	6.24	13.79
	MDWTR-D5	1163.82	7.24	10.74
Co	MDWTR-P	3.70	–	–
	MDWTR-D2	ND	–	–
	MDWTR-D5	ND	–	–
As, Cd, Hg, Pb	MDWTR-P-D2-D5	ND	–	–

Remark: The limit of detection (LOD) for all elements in ICP-OES is 0.01 mg L^{-1}.
- TMC = Total metal content.
- TCLP = Toxicity characteristic leaching procedure.
- IVBA = *In vitro* bioaccessibility (IVBA) procedure.

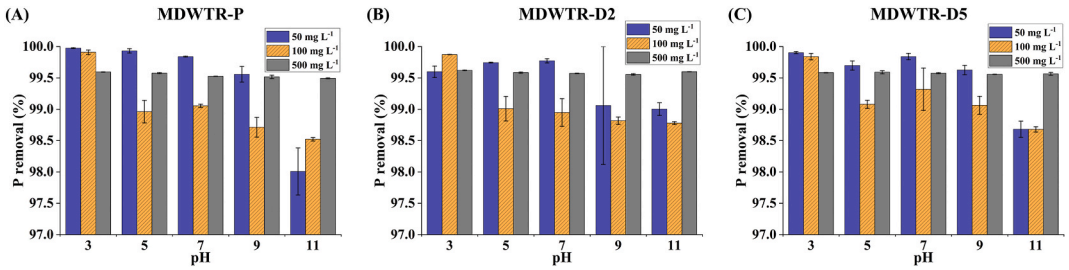

Fig. 4. The percentage of phosphorus (P) removal at different pH levels and initial P concentrations for three different materials: (A) MDWTR-P, (B) MDWTR-D2, and (C) MDWTR-D5.

3.4. Adsorption kinetics

The adsorption kinetics of phosphorus on to three different adsorbent materials (MDWTR-P, MDWTR-D2, and MDWTR-D5) were meticulously studied at varying initial phosphorus concentrations (50, 100, 250, and 500 mg L^{-1}). The experimental data were rigorously analyzed using three established kinetic models: the pseudo-first-order, pseudo-second-order, and intraparticle diffusion models. Table 4 presents the key parameters derived from these models, including the coefficient of determination (R^2) values. The pseudo-first-order model, which assumes a physisorption process, yielded a satisfactory fit to the experimental data, as evidenced by high R^2 values (ranging from 0.9005 to 0.9889) across all adsorbents and initial concentrations. However, the predicted equilibrium adsorption capacities ($q_{e,predict}$) deviated from the experimentally determined values ($q_{e,exp}$), highlighting the model's limitations in accurately describing the adsorption process. Conversely, the pseudo-second-order model, which considers chemisorption as the rate-limiting step, showed excellent agreement with the experimental data for MDWTR-P and MDWTR-D5, indicated by high R^2 values (0.9461–0.9906). For MDWTR-D2, the model exhibited a poorer fit at higher initial concentrations (250 and 500 mg L^{-1}), potentially due to the influence of other rate-limiting factors or the presence of multiple adsorption mechanisms. The intraparticle diffusion model, which assesses the contribution of intraparticle diffusion to the overall adsorption rate, demonstrated good fits ($R^2 = 0.6890$ to 0.9756) across all adsorbents and initial concentrations. This suggests that intraparticle diffusion significantly contributed to the adsorption process, particularly at higher initial concentrations, where the intraparticle diffusion rate constants (K_{diff}) were higher. Fig. 5 provides a comprehensive kinetic analysis of phosphate adsorption revealing a rapid increase in adsorption within the initial 20–30 h, followed by a gradual plateau indicating the attainment of equilibrium. The equilibrium adsorption capacity, evidenced by the plateau regions, positively correlates with the initial phosphate concentration for all three materials. Among the tested materials, MDWTR-D5 (panel C) demonstrates the highest equilibrium adsorption capacity, surpassing both MDWTR-D2 (panel B) and MDWTR-P (panel A) at all initial phosphate concentrations. Furthermore, the initial adsorption rate, inferred from the slope of the early stages of the curves, is highest for MDWTR-D5 and lowest for MDWTR-P, particularly at elevated phosphate concentrations.

3.5. Adsorption isotherm

3.5.1. Adsorption isotherm using Langmuir and Freundlich isotherm models

The results provide valuable insights into the adsorption behavior and mechanisms governing phosphorus removal by the three MDWTR materials. The Langmuir model, which assumes monolayer adsorption on to a homogeneous surface, demonstrated excellent fits to the experimental data, with high correlation coefficients ($R^2 > 0.95$) for all three adsorbents. MDWTR-D5 exhibited the highest maximum monolayer adsorption capacity ($q_m = 22.8833$ mg g^{-1}), followed by MDWTR-D2 ($q_m = 21.4133$ mg g^{-1}) and MDWTR-P ($q_m = 17.2117$ mg g^{-1}). Additionally, the Langmuir constant (K_L) for MDWTR-D5 was significantly higher (0.7199 L mg^{-1}) compared to MDWTR-D2 (0.2347 L mg^{-1}) and MDWTR-P (0.2856 L mg^{-1}), indicating a stronger affinity between MDWTR-D5 and phosphorus at each concentration. The Freundlich isotherm model, which accounts for multilayer adsorption on heterogeneous surfaces, also provided satisfactory fits to the data, with R^2 values ranging from 0.9384 to 0.9483. Notably, MDWTR-D5 exhibited the highest Freundlich adsorption capacity parameter ($K_F = 6.9720$ mg g^{-1}), indicating superior adsorption capacity compared to MDWTR-D2 ($K_F = 2.725$ mg g^{-1}) and MDWTR-P ($K_F = 2.6154$ mg g^{-1}). The Freundlich intensity parameter (1/n) values ranged from 0.7757 to 0.7929 for all three adsorbents, indicating favorable adsorption conditions. These findings suggest that phosphorus adsorption on to the MDWTR materials is governed by both monolayer and multilayer adsorption mechanisms, with MDWTR-D5 showing the highest adsorption capacity and affinity among the three adsorbents. The excellent fits obtained with both isotherm models underscore their applicability in describing the adsorption behavior and provide insights into the underlying adsorption mechanisms. Detailed results are presented in Table 5. Moreover, Fig. 6 depicts the experimental results for MDWTR-P, indicating a progressive enhancement in adsorption capacity as the equilibrium phosphate concentration increases. Both the Freundlich and Langmuir models provide satisfactory fits, while the Langmuir model demonstrates a slightly superior fit at higher concentrations. Regarding MDWTR-D2, the ability to adsorb improves significantly, and the Langmuir model provides a better fit, particularly at higher concentrations, suggesting a mostly monolayer adsorption mechanism. MDWTR-D5 demonstrates the most significant rise in adsorption capacity as the equilibrium phosphate concentration increases. The result fits the Langmuir model quite well, providing strong evidence for monolayer adsorption behavior. In general, the order of adsorption capacity is as follows: MDWTR-D5 > MDWTR-

Table 4
Kinetic parameters for phosphorus adsorption on to MDWTR-P, MDWTR-D2, and MDWTR-D5 at different initial concentrations.

Model	Parameter	Type of adsorbent/Initial concentration											
		MDWTR-P				MDWTR-D2				MDWTR-D5			
		50 mg L^{-1}	100 mg L^{-1}	250 mg L^{-1}	500 mg L^{-1}	50 mg L^{-1}	100 mg L^{-1}	250 mg L^{-1}	500 mg L^{-1}	50 mg L^{-1}	100 mg L^{-1}	250 mg L^{-1}	500 mg L^{-1}
Pseudo first order	$q_{e,exp}$ (mg L^{-1})	2.48	6.32	4.97	23.63	3.21	8.58	8.08	29.44	3.54	8.43	12.47	36.98
	K_1 (h^{-1})	0.3038	0.3349	0.3252	0.1628	0.1343	0.1522	0.3625	0.3496	0.3100	0.0486	0.3687	0.3512
	$q_{e,predict}$ (mg g^{-1})	5.67	14.37	13.54	32.51	2.90	6.24	20.62	69.11	5.77	6.05	19.97	77.62
	R^2	0.9232	0.9656	0.9005	0.9315	0.9286	0.9889	0.9712	0.9564	0.9543	0.9499	0.9261	0.9525
Pseudo second orders	K_2 (g mg^{-1} h^{-1})	0.0104	0.0102	0.0030	0.0004	0.0097	0.0085	0.0014	0.0006	0.0228	0.0132	0.0061	0.0015
	$q_{e,predict}$ (mg g^{-1})	3.50	6.02	8.10	43.67	4.38	7.76	15.06	45.66	4.12	7.75	14.86	46.08
	R^2	0.9683	0.9597	0.9461	0.9335	0.9058	0.9508	0.7368	0.7974	0.9880	0.9906	0.9571	0.9745
Intraparticle diffusion	K_{diff} (mg g^{-1} h^{-1})	0.3374	0.8575	0.7101	3.4629	0.4345	0.7543	1.2393	4.1170	0.3970	0.7211	1.5014	4.7201
	R^2	0.9701	0.9371	0.9709	0.9756	0.8320	0.9490	0.8908	0.9038	0.8545	0.9694	0.6890	0.8871

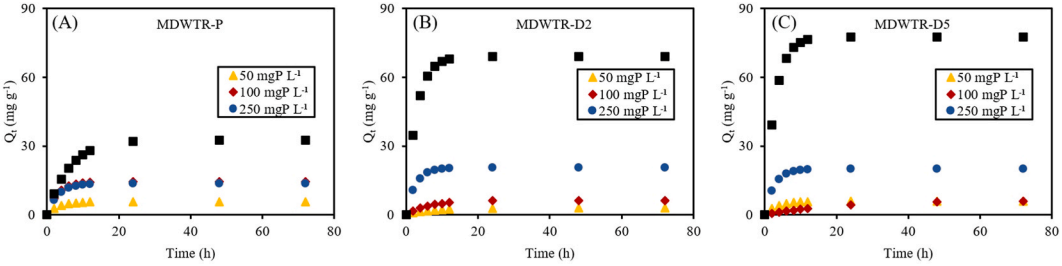

Fig. 5. The phosphorus adsorption kinetics of MDWTR materials at different initial concentrations: (A) MDWTR-P, (B) MDWTR-D2, and (C) MDWTR-D5.

Table 5
Comparison of adsorption isotherms for MDWTR-P, MDWTR-D2, and MDWTR-D5 using Langmuir and Freundlich isotherm models.

Samples	Langmuir model			Freundlich model		
	q_m (mg g^{-1})	K_L (L mg^{-1})	R^2	K_F (mg g^{-1})	1/n	R^2
MDWTR-P	17.2117	0.2856	0.9731	2.6154	0.7929	0.9483
MDWTR-D2	21.4133	0.2347	0.9570	2.725	0.7840	0.9447
MDWTR-D5	22.8833	0.7199	0.9610	6.9720	0.7757	0.9384

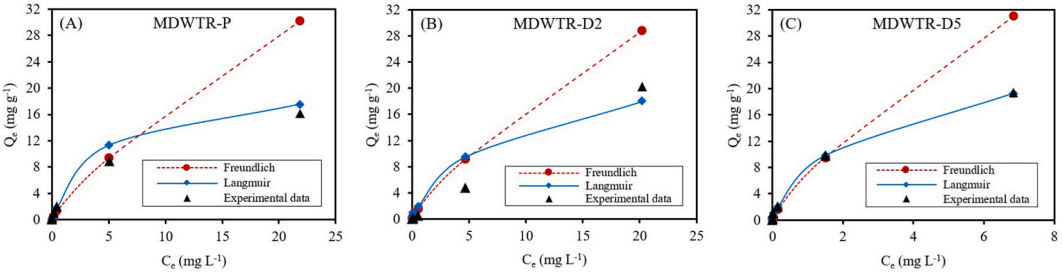

Fig. 6. Adsorption isotherm plots for (A) MDWTR-P, (B) MDWTR-D2, and (C) MDWTR-D5.

D2 > MDWTR-P. This indicates that MDWTR-D5 has the greatest affinity for phosphate adsorption.

3.5.2. Comparative analysis of phosphorus concentrations in adsorption experiments using one way ANOVA

Table 6 presents a thorough statistical analysis of phosphorus levels in several groups of MDWTR samples. The study shows significant differences, which strengthens the credibility of these findings. The study of MDWTR-P results in the outcome ($F(4,10) = 2.7 \times 10^5$, p-value <0.001), demonstrating significant variations in phosphorus concentrations among the groups. For MDWTR-D2 the outcome is ($F(4,10) = 1.2 \times 10^6$, p-value <0.001), indicating highly significant changes in phosphorus concentrations between the groups. Similarly, for MDWTR-D5 the outcome is ($F(4,10) = 3.2 \times 10^5$, p-value <0.001), which confirms that there are substantial differences in phosphorus concentrations between the groups. The F-statistics, which are very significant, along with the very low p-values, highlight the strength and dependability of our data. Additionally, Table 7 provides a comprehensive overview of pairwise comparisons of mean phosphorus concentrations following a 72-h adsorption period with an initial concentration of 200 mg P, across

Table 6
A one way ANOVA method was used to conduct a comparative analysis of the ultimate phosphorus concentrations in adsorption experiments with MDWTR-P, MDWTR-D2, and MDWTR-D5. The initial concentrations of phosphorus were 2, 10, 20, 100, and 200 mg.

MDWTR types	Sources	df	Sum of square	Mean square	F	p
MDWTR-P	Between groups	4	3505.9526	876.4881	2.7e+05	<0.001
	Within groups	10	0.0319	0.0032		
	Total	14	3505.9845	250.4275		
MDWTR-D2	Between groups	4	901.0594	225.2648	1.2e+06	<0.001
	Within groups	10	0.0019	0.0002		
	Total	14	901.0613	64.3615		
MDWTR-D5	Between groups	4	103.7071	25.9268	3.2e+05	<0.001
	Within groups	10	0.0008	0.0001		
	Total	14	103.7079	7.4077		

Table 7
Pairwise comparisons of mean phosphorus concentrations after 72-h adsorption with 200 mg P initial concentrations between MDWTR-P, MDWTR-D2, and MDWTR-D5.

MDWTR types	Mean difference	Std. error	95 % Conf. Interval		p
			Upper	Lower	
MDWTR-D2 Vs MDWTR-P	−19.4237	0.0259	−19.5033	−19.3442	<0.001
MDWTR-D5 Vs MDWTR-P	−32.7954	0.0259	−32.8749	−32.7159	<0.001
MDWTR-D5 Vs MDWTR-D2	−13.3716	0.0259	−13.4512	−13.2921	<0.001

three distinct material types: MDWTR-P, MDWTR-D2, and MDWTR-D5. Each comparison reveals statistically significant differences (p-value <0.001) in mean phosphorus concentrations between the materials, indicating robust variations in their adsorption capabilities. Specifically, MDWTR-D2 exhibits a mean difference of −19.4237 (95 % CI: 19.5033, −19.3442) compared to MDWTR-P, while MDWTR-D5 displays a substantially greater difference of −32.7954 (95 % CI: 32.8749, −32.7159) relative to MDWTR-P. Moreover, the comparison between MDWTR-D5 and MDWTR-D2 reveals a moderate difference of −13.3716 (95 % CI: 13.4512, −13.2921). The inclusion of standard errors in the table enhances the reliability of these findings, providing a robust statistical basis for assessing the distinct adsorption performances of the MDWTR materials.

4. Discussion

4.1. The implications of metal composition, structural attributes, and pH on the adsorption effectiveness

The notable differences in metal concentrations found in MDWTR samples through Total Metal Concentration (TMC) analysis underscore the critical importance of understanding the role these metals play in phosphorus adsorption and their overall environmental impact [43]. Specifically, the discovery that MDWTR-P has the highest TMC for aluminum, while MDWTR-D5 shows elevated TMC values for iron, calcium, and manganese, highlights the diverse composition of MDWTR materials and their varying safety profiles [44]. Additionally, the Toxicity Characteristic Leaching Procedure (TCLP) assessment reveals potential concerns for groundwater contamination and regulatory compliance, as evidenced by MDWTR-P's increased release of calcium, iron, and aluminum under simulated environmental conditions. To provide context, the U.S. Environmental Protection Agency (EPA) has established regulatory limits for various metals in TCLP extracts to determine if a waste product is hazardous [45]. For instance, the EPA limit for lead is 5 mg L^{-1}, while for cadmium it is 1 mg L^{-1} [46]. Although the TCLP results for MDWTR samples do not exceed these specific limits, the elevated levels of aluminum and iron in MDWTR-P (1383.00 mg L^{-1} and 65.33 mg L^{-1}, respectively) warrant careful consideration in terms of potential environmental impacts [45,46]. Furthermore, the *in vitro* bioaccessibility (IVBA) analysis demonstrates significant variations in metal bioavailability, with MDWTR-P exhibiting higher bioaccessibility percentages compared to MDWTR-D2 and MDWTR-D5, indicating different levels of risk associated with metal exposure. While there are no universally accepted standards for IVBA results, these findings are crucial for assessing potential health risks. For example, the bioaccessibility of aluminum in MDWTR-P (7.48 %) is notably higher than in MDWTR-D2 (5.12 %) and MDWTR-D5 (6.02 %), suggesting a greater potential for aluminum uptake from MDWTR-P. These findings underscore the necessity of considering metal composition, bioaccessibility, and leachability when assessing the environmental suitability and potential risks of using MDWTR materials, particularly in phosphorus adsorption applications and broader environmental management strategies [47,48]. The study's results on the leachability and bioaccessibility of metals in MDWTR forms have significant implications for environmental safety and regulatory policies. The absence of toxic metals in MDWTR-D2 and MDWTR-D5, combined with their lower leachability and bioaccessibility, suggests these forms may be more suitable for long-term application, posing fewer environmental risks. These insights can inform policymakers and regulatory agencies in setting standards and guidelines for the safe use of MDWTR in wastewater treatment. To support evidence-based decision-making and mitigate potential negative effects on ecosystems and human health, further investigation into the mechanisms underlying metal-phosphorus interactions and their implications for water treatment and environmental stewardship is warranted [49].

The surface area results, meticulously derived using a comprehensive suite of analytical methods including Single Point BET, Multi Point BET, Langmuir surface area, and BJH cumulative adsorption [50,51], consistently demonstrate that MDWTR-D5 exhibits the largest surface area, with values ranging from 39.53 $m^2\ g^{-1}$ (as determined by the BJH method) to 284.7 $m^2\ g^{-1}$ (as determined by the Langmuir method). This remarkable consistency across diverse measurement techniques not only reinforces the reliability and accuracy of our findings but also underscores the suitability of MDWTR-D5 for applications necessitating extensive surface interactions, such as catalysis and adsorption [52]. The rigorous methodological approach employed ensures that the results are both robust and reproducible, providing a high degree of confidence in the material's potential performance [53,54].

In terms of pore volume, MDWTR-D2 is distinguished by its superior overall pore volume of 0.2119 $cm^3\ g^{-1}$ and BJH cumulative adsorption pore volume of 0.1934 $cm^3\ g^{-1}$. This significant pore volume is indicative of enhanced adsorption capacities, positioning MDWTR-D2 as a highly promising candidate for applications where pore volume is a critical determinant of performance. The precision of these measurements, obtained through well-established techniques, further substantiates the material's potential efficacy in relevant applications. Conversely, the micropore volume of MDWTR-D5, quantified at 0.0448 $cm^3\ g^{-1}$ via the HK technique, highlights its potential for applications that require adsorption within smaller pore structures [58]. This finding is supported by the meticulous application of the HK method, ensuring the reliability of the micropore volume data. The pore size analysis provides additional

insights, revealing that MDWTR-P possesses the largest average pore radius of 57.2 Å, which could be advantageous for processes involving larger molecular entities [56]. Despite this, the consistent BJH adsorption pore radii (approximately 17.99 Å) and HK method pore radii (1.838 Å) observed across all materials suggest a uniformity in pore size distribution. This uniformity can be particularly beneficial for applications that demand consistent pore characteristics, enhancing the predictability and reliability of the materials' performance in practical applications.

The study on the impact of pH on phosphorus adsorption by Modified Drinking Water Treatment Residuals (MDWTRs) provides important information on the effectiveness of phosphorus removal in water treatment [57]. The study confirms the reliable adsorption abilities of MDWTR materials in removing phosphorus. This is demonstrated through a thorough evaluation of MDWTR-P, MDWTR-D2, and MDWTR-D5 at different pH levels and baseline phosphorus concentrations. The results consistently show that MDWTR materials are highly effective in removing phosphorus, making them a promising option for phosphorus removal [51,55,59]. Remarkably, MDWTR-P and MDWTR-D2 demonstrated outstanding removal rates surpassing 98 % throughout a wide range of pH levels, whereas MDWTR-D5 revealed slightly lower but still noteworthy removal efficiency. The results highlight the effectiveness of MDWTR in removing phosphorus, especially at pH levels of around 5 and 7. This indicates that MDWTRs are suitable for practical use in water treatment procedures to combat phosphorus contamination in aquatic ecosystems. Additional investigation into the fundamental mechanisms that control the adsorption behavior of MDWTRs under different pH conditions shows potential for enhancing its effectiveness in environmental clean-up endeavors [60,61].

4.2. Adsorption kinetics and adsorption isotherm

4.2.1. Adsorption kinetics

The study conducted a thorough examination of the adsorption kinetics of phosphorus on to three distinct MDWTR materials (MDWTR-P, MDWTR-D2, and MDWTR-D5) at different initial phosphorus concentrations (50, 100, 250, and 500 mg L^{-1}). This investigation yielded valuable academic insights into the factors that affect the efficiency of phosphorus removal [28]. The study's meticulous analysis of three proven kinetic models, including pseudo-first-order, pseudo-second-order, and intraparticle diffusion provides insight into the complex mechanisms of phosphorus adsorption by these materials [62,63]. The pseudo-first-order model, supposing a physical absorption process, produced strong R^2 values (ranging from 0.9005 to 0.9889) for all adsorbents and beginning concentrations, showing a satisfactory agreement with the experimental results [64]. Nevertheless, the disparities between the anticipated equilibrium adsorption capabilities (q_e,predict) and the values established through experimentation (q_e,exp) highlight the model's constraints in comprehensively capturing the intricacies of the adsorption process [65].

In contrast, the pseudo-second-order model, which takes into account chemisorption as the step that limits the rate, showed a strong agreement with experimental results for MDWTR-P and MDWTR-D5. The R^2 values ranged from 0.9461 to 0.9906, indicating that chemisorption plays a substantial part in the adsorption processes of these compounds. Nevertheless, the lower accuracy reported for MDWTR-D2 at higher starting concentrations (250 and 500 mg L^{-1}) suggests the potential existence of other elements that restrict the rate, or numerous mechanisms of adsorption that are influencing its effectiveness [66]. The intraparticle diffusion model yielded strong fits (R^2 = 0.6890 to 0.9756) for all adsorbents and starting concentrations, indicating the significant role of intraparticle diffusion in the overall adsorption process [67] along with reports of larger intraparticle diffusion rate constants (K_{diff}) at higher starting concentrations, indicating a clear relationship between the two variables. An extensive kinetic investigation demonstrated a fast augmentation in adsorption over the first 20–30 h, succeeded by a steady stabilization indicating the achievement of equilibrium [68]. The adsorption capacity at equilibrium, as indicated by these plateau regions, exhibited a positive connection with the initial concentration of phosphate for all three materials. MDWTR-D5 exhibited the greatest equilibrium adsorption capacity among the investigated adsorbents, surpassing both MDWTR-D2 and MDWTR-P, across all initial phosphate concentrations. In addition, the pace at which the adsorption process first occurs, as determined by the early slope of the adsorption curves, was shown to be highest for MDWTR-D5 and lowest for MDWTR-P, especially when phosphate concentrations were high. The discovered patterns were consistently present in many experimental configurations, enhancing the dependability of the results. These findings have substantial scholarly ramifications. The superior fit of the pseudo-second-order model for MDWTR-P and MDWTR-D5 indicates that improving chemisorption processes could increase the efficiency of phosphorus removal [69]. The significance of intraparticle diffusion, particularly at elevated concentrations, emphasizes the necessity to take into account both surface and pore diffusion mechanisms in the development and utilization of these materials [70]. The exceptional performance of MDWTR-D5 demonstrates its capacity as a remarkably efficient adsorbent for phosphorus removal, offering a promising alternative for water treatment applications [71]. To summarize, this study enhances our comprehension of the adsorption mechanisms of MDWTR materials and emphasizes the significance of taking into account both kinetic and diffusion aspects in order to optimize their performance for phosphorus removal. The knowledge acquired from this research can guide the creation of more efficient water treatment methods, hence enhancing environmental management and attempts to reduce pollution [72]. The meticulous methodology and comprehensive validation of the outcomes guarantee the dependability and relevance of these findings in practical situations.

4.2.2. Adsorption isotherm

The comprehensive investigation of adsorption isotherms through the utilization of the Langmuir and Freundlich models has significant scientific implications in comprehending the mechanisms that regulate the elimination of phosphorous by Modified Drinking Water Treatment Residuals (MDWTRs). The Langmuir model, which posits that adsorption occurs in a single layer on a uniform surface, provided highly accurate fits to the experimental data. The correlation coefficients (R^2) for all three adsorbents were above 0.95, indicating a strong relationship between the model and the data. The model's assumptions are highly reliable, as

evidenced by the good fit. This indicates that phosphorus adsorption on to MDWTRs mainly happens as a monolayer on a uniform surface [73]. MDWTR-D5 had the highest maximal monolayer adsorption capacity (q_m = 22.8833 mg g^{-1}) among the investigated materials, surpassing MDWTR-D2 (q_m = 21.4133 mg g^{-1}) and MDWTR-P (q_m = 17.2117 mg g^{-1}) by a large margin. The higher capacity and much larger Langmuir constant (K_L = 0.7199 L mg^{-1}) of MDWTR-D5, compared to MDWTR-D2 (K_L = 0.2347 L mg^{-1}) and MDWTR-P (K_L = 0.2856 L mg^{-1}), suggest a stronger attraction between MDWTR-D5 and phosphorus at all tested concentrations. In addition, the Freundlich isotherm model, which considers the adsorption of many layers on surfaces with different properties, also showed good fits with R^2 values ranging from 0.9384 to 0.9483 [74]. MDWTR-D5 exhibited the greatest Freundlich adsorption capacity parameter (K_F = 6.9720 mg g^{-1}), significantly surpassing the values for MDWTR-D2 (K_F = 2.725 mg g^{-1}) and MDWTR-P (K_F = 2.6154 mg g^{-1}). The Freundlich intensity parameter (1/n) values for the three adsorbents ranged from 0.7757 to 0.7929, demonstrating favorable adsorption conditions and supporting the feasibility of these materials for practical use in different environmental contexts. The elucidation of phosphorus adsorption mechanisms by MDWTRs was achieved through a rigorous analysis of elemental composition changes before and after adsorption, utilizing XRF and SEM-EDS techniques. This multi-analytical approach revealed a complex interplay of concurrent processes, including ion exchange, surface precipitation, surface complexation, and electrostatic interactions, consistent with the established literature. Ion exchange [75,76] was evidenced by significant decreases in calcium (22.02 %), magnesium (4.49 %), and sulfur (54.55 %) content, coupled with increases in potassium (17.99 %). Surface precipitation [77] was indicated by increased iron content (11.62 %) and substantial phosphorus uptake (1042.86 %) for MDWTR-D2. Surface complexation was inferred from changes in aluminum and iron content [78], while electrostatic interactions were supported by overall compositional changes [79]. The superior performance of MDWTR-D5, attributed to its stable structure (minimal changes in Al and Si content), aligns with findings on high-performance adsorbents. This comprehensive approach, integrating macroscopic isotherm data (Langmuir $R^2 > 0.95$, Freundlich $R^2 > 0.93$) with microscopic elemental changes, provides a nuanced understanding of adsorption mechanisms, offering valuable insights for optimizing phosphorus removal strategies in water treatment applications, while a comparative analysis of MDWTRs with alternative phosphorus removal methods reveals both promising aspects and challenges. MDWTRs demonstrate high phosphorus adsorption efficiency [80], cost-effectiveness due to waste material utilization [81], and alignment with circular economy principles [82]. However, they face scalability issues and potential metal leaching concerns [83]. Traditional chemical precipitation, while efficient, produces significant sludge and risks secondary pollution [84]. Biological methods like Enhanced Biological Phosphorus Removal (EBPR) offer natural processes but require specific conditions and longer retention times [85]. Other adsorbents such as activated carbon or biochar are cost-effective but may struggle with regeneration and throughput [86]. MDWTRs show competitive efficiency and lower environmental impact compared to chemical methods [87], simpler operation than biological approaches [88], and potential for phosphorus recovery [89]. The analysis employed one way ANOVA to compare phosphorus concentrations among MDWTR groups and independence assumptions. The extremely low p-values (<0.001) for MDWTR-P, MDWTR-D2, and MDWTR-D5, coupled with large F-statistics, provide strong evidence against the null hypothesis of no difference among group means. These results indicate statistically significant differences in phosphorus concentrations among the groups for each MDWTR type. Pairwise comparisons using post-hoc tests (Tukey's HSD) further support these findings, with all comparisons yielding p-values <0.001. The narrow 95 % confidence intervals and small standard errors reported for these comparisons suggest high precision in our estimates of differences between MDWTR types. This comprehensive statistical approach, including careful consideration of ANOVA assumptions, interpretation of p-values in the context of hypothesis testing, and detailed pairwise comparisons, provides robust evidence for significant differences in phosphorus adsorption capabilities among the MDWTR materials studied, enhancing the reliability and significance of our findings.

To summarize, the adsorption capacity follows the order MDWTR-D5 > MDWTR-D2 > MDWTR-P, indicating that MDWTR-D5 has the highest affinity for phosphate adsorption. Notably, MDWTR-D5 exhibits exceptional promise for phosphorus removal in water treatment applications, attributed to its high iron content (87,519.07 mg kg^{-1}) coupled with low leachability and *in vitro* bioaccessibility (IVBA) [90,91]. This characteristic suggests MDWTR-D5 could effectively mitigate eutrophication risks in aquatic ecosystems without introducing significant quantities of iron into the environment.

However, the environmental implications of MDWTR application warrant careful consideration. The high aluminum content and leachability observed in MDWTR-P (TMC: 170,165.68 mg kg^{-1}; TCLP: 1383.00 mg L^{-1}) raise concerns about potential toxicity to aquatic organisms [92]. Elevated aluminum levels in aquatic environments have been associated with detrimental effects on fish gill function and overall ecosystem health [93]. This underscores the necessity for rigorous pre-application assessment and ongoing monitoring of MDWTR use, particularly in sensitive aquatic habitats. The variability in metal leaching potential among MDWTR samples highlights a critical limitation. While MDWTR-D5 and MDWTR-D2 demonstrate relatively low metal leachability, the high aluminum leachability of MDWTR-P could pose significant environmental risks in certain applications. This variability necessitates careful characterization and selection of MDWTRs based on their specific compositional profiles and the intended application environment.

5. Conclusion

In this study, MDWTRs were investigated for their potential in phosphorus removal from water. Three types of MDWTR materials - MDWTR-P, MDWTR-D2, and MDWTR-D5 - were extensively characterized and evaluated for their phosphorus adsorption capabilities. The experimental results demonstrated that MDWTR materials, particularly MDWTR-D5, exhibit excellent phosphorus adsorption capacity, with maximum monolayer adsorption capacities reaching 22.8833 mg g^{-1} for MDWTR-D5.

The comprehensive characterization of MDWTR materials revealed significant differences in their metal compositions and structural attributes. MDWTR-D5 showed the highest surface area, ranging from 39.53 to 284.7 m^2 g^{-1}, while MDWTR-D2 exhibited the

largest overall pore volume of 0.2119 $cm^3\ g^{-1}$. These characteristics contributed to their adsorption performance, with MDWTR-D5 demonstrating superior phosphorus removal efficiency across various experimental conditions. Kinetic model analysis indicated that the adsorption process for MDWTR-P and MDWTR-D5 primarily followed the pseudo-second-order model, suggesting chemisorption as the dominant mechanism. The adsorption isotherms were best described by both the Langmuir and Freundlich models, with high correlation coefficients ($R^2 > 0.95$ for Langmuir and $R^2 > 0.93$ for Freundlich), indicating a complex adsorption process involving both monolayer and multilayer adsorption. The study revealed that MDWTR materials exhibited high phosphorus removal efficiency (>98 %) across a wide pH range, with optimal performance at pH 5 and 7. This demonstrates their adaptability and reliability under different environmental conditions. The adsorption mechanisms were elucidated through elemental composition analysis, revealing a complex interplay of ion exchange, surface precipitation, surface complexation, and electrostatic interactions. Environmental implications were carefully considered, with MDWTR-D5 showing promising potential for phosphorus removal with low environmental risk due to its high iron content coupled with low leachability and *in vitro* bioaccessibility. However, concerns were raised regarding MDWTR-P due to its high aluminum leachability, highlighting the importance of material selection based on specific compositional profiles and intended application environments.

In summary, this study successfully characterized and evaluated MDWTR materials for phosphorus adsorption, demonstrating their significant potential for water treatment applications. The research provides valuable insights into the adsorption mechanisms and environmental implications of MDWTR use. While this study focused on comprehensive material characterization and adsorption performance under various conditions, future research should prioritize the evaluation of MDWTR materials' regeneration capacity and long-term stability under diverse environmental conditions. Furthermore, to bridge the gap between laboratory findings and practical implementation, strongly advocation for the establishment of strategic collaborations between academic research institutions and industry partners is necessary. Such alliances would facilitate knowledge transfer, expedite pilot-scale testing, and accelerate the path to commercial implementation.

Data availability

Data will be made available on request.

Funding

This research was generously supported by Ubon Ratchathani University.

CRediT authorship contribution statement

Sitthichai Chaikhan: Writing – original draft, Visualization, Methodology, Investigation, Formal analysis, Data curation, Conceptualization. **Somjate Thongdamrongtham:** Writing – review & editing, Supervision, Project administration, Methodology, Investigation, Funding acquisition, Data curation, Conceptualization. **Supanee Junsiri:** Methodology, Investigation, Data curation. **Chiraporn Labcom:** Writing – review & editing, Methodology, Formal analysis. **Anootsara Sarak:** Project administration, Methodology, Investigation. **Laksanee Boonkhao:** Validation, Methodology.

Declaration of competing interest

The authors declare that none of the work reported in this study could have been influenced by any known competing financial interests or personal relationships.

Acknowledgment

The research was carried out on behalf of the executive officers and regional authorities, with funding support from Ubon Ratchathani University. The Office of Physical and Environmental Management, which assisted in collecting water samples, collaborated on the project. The Ubon Ratchathani Provincial Waterworks Authority has supplied DWTR samples for scientific investigation.

References

[1] K.W. Jung, M.J. Hwang, K. Kim, K.H. Ahn, Adsorption of phosphate from aqueous solution on to pyrolyzed drinking water treatment residuals: statistical process optimization, equilibrium, and kinetic analysis, Environ. Prog. Sustain. Energy 35 (4) (2014) 1035–1046, https://doi.org/10.1002/ep.12319.
[2] R. Viviani, Eutrophication, marine biotoxins, human health, Sci. Total Environ. (1992) 631–662, https://doi.org/10.1016/b978-0-444-89990-3.50056-0.
[3] N. Prathumchai, C. Polprasert, A.J. Englande, Phosphorus leakage from fisheries sector – a case study in Thailand, Environ. Pollut. 219 (2016) 967–975, https://doi.org/10.1016/j.envpol.2016.09.081.
[4] B.T.G. Balasuriya, A. Ghose, S.H. Gheewala, T. Prapaspongsa, Assessment of eutrophication potential from fertiliser application in agricultural systems in Thailand, Sci. Total Environ. 833 (2022) 154993, https://doi.org/10.1016/j.scitotenv.2022.154993.
[5] M. Wildemeersch, S. Tang, T. Ermolieva, Y. Ermoliev, E. Rovenskaya, M. Obersteiner, Containing the risk of phosphorus pollution in agricultural watersheds, Sustainability 14 (3) (2020) 1717, https://doi.org/10.3390/su14031717.
[6] Y. Tong, X. Wang, J.J. Elser, Unintended nutrient imbalance induced by wastewater effluent inputs to receiving water and its ecological consequences, Front. Environ. Sci. Eng. 16 (11) (2022) 149, https://doi.org/10.1007/s11783-022-1584-x.

[7] K. Thongkao, K. Suwannahong, P. Sangmek, The integration of europhication and water quality monitoring for planning of domestic wastewater management in urban model, Bangkok, Thailand, in: ACM International Conference Proceeding Series, Association for Computing Machinery, Mar. 2019, pp. 83–87, https://doi.org/10.1145/3323716.3323761.

[8] R.K. Mishra, The effect of eutrophication on drinking water, Br. J. Multidiscip. Adv. Stud. 4 (1) (2023) 7–20, https://doi.org/10.37745/bjmas.2022.0096.

[9] A. Ural-Janssen, C. Kroeze, M. Strokal, Reducing future coastal eutrophication under global change in Europe, EGU Gen. Assem. 23 (2023) EGU23–6212, https://doi.org/10.5194/egusphere-egu23-6212.

[10] A. Nakarmi, S. Kanel, M.N. Nadagouda, T. Viswanathan, Chapter 7 - applications of conventional and advanced technologies for phosphorus remediation from contaminated water, in: U. Shanker, C.M. Hussain, M. Rani (Eds.), Green Functionalized Nanomaterials for Environmental Applications, Elsevier, Amsterdam, 2022, pp. 181–213.

[11] A.I. Velásquez, A.K. Zipa, S.D. Cevallos, C. Marina-Montes, J.M. Anzano, Precipitation of orthophosphate in a wastewater treatment plant. Water, Air. Soil. Pollut. 232 (4) (2021) 126, https://doi.org/10.1007/s11270-021-05077-4.

[12] H. Cavalcante, F. Araújo, V. Becker, J.E. Lucena-Barbosa, Control of internal phosphorus loading using coagulants and clays in water and the sediment of a semiarid reservoir susceptible to resuspension, Hydrobiologia 849 (2022) 4059–4071, https://doi.org/10.1007/s10750-021-04737-0.

[13] A. Cainglet, H. Postila, P. Rossi, E. Heiderscheidt, Coagulant precipitated and biologically stabilized sewage sludge impacts nutrient availability, and risk of nutrient and micropollutant leaching in sludge-amended soils, EGU Gen. Assem. 23 (2023) EGU23–14857, https://doi.org/10.5194/egusphere-egu23-14857.

[14] M. Dolatabadi, H. Naidu, S. Ahmadzadeh, A green approach to remove acetamiprid insecticide using pistachio shell-based modified activated carbon; economical groundwater treatment, J. Cleaner. Prod. 316 (2021) 128226, https://doi.org/10.1016/j.jclepro.2021.128226.

[15] R. Rahmati, V. Sidhu, R. Nunez, R. Datta, D. Sarkar, Correlation of phosphorus adsorption with chemical properties of aluminum-based drinking water treatment residuals collected from various parts of the United States, Molecules 27 (21) (2022) 7194, https://doi.org/10.3390/molecules27217194, 7194.

[16] Y. Zhao, C. Wang, L.A. Wendling, Y. Pei, Feasibility of using drinking water treatment residuals as a novel chlorpyrifos adsorbent, J. Agric. Food Chem. 61 (31) (2013) 7446–7452, https://doi.org/10.1021/jf401763f.

[17] M. Año Soto, P. Almenar, J. Macián, Safe T WATER : an eco-sustainable technology to replace aluminum salts with natural coagulants, EGU Gen. Assem. 23 (2023) EGU23–6670, https://doi.org/10.5194/egusphere-egu23-6670.

[18] L. Shi, X. Zhao, Y. Cao, H. Ma, X. Sun, Physicochemical properties and phosphorus adsorption capacity of ceramsite made from alum sludge, Water 15 (13) (2023) 2427, https://doi.org/10.3390/w15132427.

[19] M. Pająk, Alum sludge as an adsorbent for inorganic and organic pollutants removal from aqueous solutions: a review, Int. J. Environ. Sci. Technol. 20 (10) (2023) 10953–10972. https://doi:10.1007/s13762-023-04854-4.

[20] R. Duan, C.B. Fedler, Modeling phosphorus adsorption onto polyaluminium chloride water treatment residuals, Water. Sci. Technol. Water. Supply. 21 (1) (2021) 458–469, https://doi.org/10.2166/ws.2020.322.

[21] K.C. Makris, W.G. Harris, G.A. O'Connor, T.A. Obreza, H.A. Elliott, Physicochemical properties related to long-term phosphorus retention by drinking-water treatment residuals, Environ. Sci. Technol. 39 (11) (2005) 4280–4289, https://doi.org/10.1021/es0480769.

[22] A.C. Kuster, B.J. Huser, S. Padungthon, R. Junggoth, A.T. Kuster, Washing and heat treatment of aluminum-based drinking water treatment residuals to optimize phosphorus sorption and nitrogen leaching: considerations for lake restoration, Water 13 (18) (2021) 2465, https://doi.org/10.3390/w13182465.

[23] A.M. Mahdy, E. Elkhatib, T. Zhang, N.O. Fathi, Z.Q. Lin, Nano-scale drinkingwater treatment residuals affect arsenic fractionation and speciation in biosolids-amended agricultural soil, Appl. Sci. 10 (16) (2020) 5633, https://doi.org/10.3390/app10165633.

[24] M. Wołowiec, M. Komorowska-Kaufman, A. Pruss, G. Rzepa, T. Bajda, Removal of heavy metals and metalloids from water using drinking water treatment residuals as adsorbents: a review, Minerals 9 (8) (2019) 487, https://doi.org/10.3390/min9080487.

[25] M.M. Nour, M.A. Tony, H.A. Nabwey, Adsorptive pattern using drinking water treatment residual for organic effluent abatement from aqueous solutions, Materials 16 (1) (2023) 247, https://doi.org/10.3390/ma16010247.

[26] M.R. Ament, E.D. Roy, Y. Yuan, S.E. Hurley, Phosphorus removal, metals dynamics, and hydraulics in stormwater bioretention systems amended with drinking water treatment residuals, J. Sustain. Water Built Environ. 8 (3) (2022) 04022003, https://doi.org/10.1061/jswbay.0000980.

[27] G. Fu, Y. Zhao, S. Zhou, C. Chen, Y. Zhong, Y. Xu, Efficient removal of nitrogen and phosphorus in aqueous solutions using modified water treatment residuals–sodium alginate beads, Environ. Sci. Pollut. Res. 28 (34) (2021) 46233–46246, https://doi.org/10.1007/s11356-021-12586-6.

[28] X. Li, J. Cui, Y. Pei, Granulation of drinking water treatment residuals as applicable media for phosphorus removal, J. Environ. Manag. 213 (2018) 36–46, https://doi.org/10.1016/j.jenvman.2018.02.056.

[29] O. Juntarasakul, M. Rawangphai, T. Phengsaart, K. Maneeintr, Influences and isotherm models on phosphorus removal from wastewater by using Fe^{3+}-type UBK10 cation exchange resin as absorbent, Metals 13 (7) (2023) 1166, https://doi.org/10.3390/met13071166.

[30] X. Wu, R. Zhan, L. Liu, J. Lan, N. Zhao, Z. Wang, Phosphorus adsorption on blast furnace slag with different magnetism and its potential for phosphorus recovery, Water 14 (16) (2022) 2452, https://doi.org/10.3390/w14162452.

[31] W. Brontowiyono, et al., Phosphate ion removal from synthetic and real wastewater using $MnFe_2O_4$ nanoparticles: a reusable adsorbent, Acta Chim. Slov. 69 (3) (2022) 681–693, https://doi.org/10.17344/acsi.2022.7594.

[32] M. Wei, X. Duan, W. Zhou, K. Huang, Y. Chen, J. Tie, Enhanced Adsorption of two reactive dyes onto Al-based waterworks sludge modified by calcination, Pol. J. Environ. Stud. 32 (3) (2023) 2373–2381, https://doi.org/10.15244/pjoes/159080.

[33] J. Šarko, T. Leonavičienė, A. Mažeikienė, Research and modelling the ability of waste from water and wastewater treatment to remove phosphates from water, Processes 10 (2) (2022) 412, https://doi.org/10.3390/pr10020412.

[34] E. Nabatian, M. Dolatabadi, S. Ahmadzadeh, Application of experimental design methodology to optimize acetaminophen removal from aqueous environment by magnetic chitosan@multi-walled carbon nanotube composite: isotherm, kinetic, and regeneration studies, Anal. Methods Environ. Chem. J. 5 (1) (2022) 61–74, https://doi.org/10.24200/amecj.v5.i01.168.

[35] S. Ahmadzadeh, M. Dolatabad, R. Malekahmadi, A. Rasooli, Quantum dots and their application in water and wastewater treatment, J. Environ. Health Sustain. Dev. 8 (1) (2023) 1862–18624, https://doi.org/10.18502/jehsd.v8i1.12317.

[36] M. Dolatabadi, A. Ghorbanian, S. Ahmadzadeh, Mg-Al–layered double hydroxide as promising sustainable nanoadsorbent for application in water/wastewater treatment processes; diethyl phthalate removal, J. Environ. Health Sustain. Dev. 6 (3) (2021) 1367–1375, https://doi.org/10.18502/jehsd.v6i3.7244.

[37] S. Thongdamrongtham, S. Junsiri, N. Mongkol, S. Chaikhan, A breakthrough approach for superior cyanobacteria (*Microcystis aeruginosa*) removal and phosphorus adsorption, Ecol. Eng. Environ. Technol. 25 (2) (2024) 333–350, https://doi.org/10.12912/27197050/177133.

[38] K.W. Jung, M.J. Hwang, T.U. Jeong, D.M. Chau, K. Kim, K.H. Ahn, Entrapment of powdered drinking water treatment residues in calcium-alginate beads for fluoride removal from actual industrial wastewater, J. Ind. Eng. Chem. 39 (2016) 101–111, https://doi.org/10.1016/j.jiec.2016.05.017.

[39] U.S. EPA, Standard Operating Procedure for an in Vitro Bioaccessibility Assay for Lead in Soil, 2012. EPA 9200.2-86).

[40] APHA, in: E.W. Rice, L. Bridgewater (Eds.), American Public Health Association, American Water Works Association, Standard Methods for the Examination of Water and Wastewater, Water Environment Federation, American Public Health Association, Washington, D.C., 2012.

[41] S. Azizian, Kinetic models of sorption: a theoretical analysis, J. Colloid Interface Sci. 276 (1) (2004) 47–52, https://doi.org/10.1016/j.jcis.2004.03.048.

[42] H. Fakour, T.F. Lin, Effect of humic acid on as redox transformation and kinetic adsorption onto iron oxide based adsorbent (IBA), Int. J. Environ. Res. Public Health. 11 (10) (2014) 10710–10736, https://doi.org/10.3390/ijerph111010710.

[43] E. Lombi, D.P. Stevens, M.J. McLaughlin, Effect of water treatment residuals on soil phosphorus, copper and aluminium availability and toxicity, Env. Pol. 158 (6) (2010) 2110–2116, https://doi.org/10.1016/j.envpol.2010.03.006.

[44] S. Sharma M.M. Ahammed, Application of modified water treatment residuals in water and wastewater treatment: a review, Heliyon 9 (5) (2023) e15796, https://doi.org/10.1016/j.heliyon.2023.e15796.

[45] US EPA, TCLP requirements for the method of standard addition. https://archive.epa.gov/epawaste/hazard/web/html/faq_tclp.html, 2016. (Accessed 31 August 2024).

[46] ALS Global's Global Headquarters, Australia, EPA limits for RCRA 8 metals. https://www.alsglobal.com/en/news-and-publications/2023/10/rcra-8-metals-guide, 2023. (Accessed 31 August 2024).
[47] M. Kasprzyk, K. Czerwionka, M. Gajewska, Waste materials assessment for phosphorus adsorption toward sustainable application in circular economy, Resour. Conserv. Recycl. 168 (2021) 105335, https://doi.org/10.1016/j.resconrec.2020.105335.
[48] Y. Zhang, C. Shan, J. Qian, B. Pan, Scenario oriented strategies for phosphorus management by using environmental nanotechnology, Curr. Opin. Chem. Eng. 34 (2021) 100720, https://doi.org/10.1016/j.coche.2021.100720.
[49] K.A.H. Arab, D.F. Thompson, I.W. Oliver, Evaluation and characterisation of metal sorption and retention by drinking water treatment residuals (WTRs) for environmental remediation, I, J. Environ. Sci. Technol. 19 (8) (2021) 1–10, https://doi.org/10.1007/s13762-021-03674-8.
[50] L.W. He, Y. Chen, F. Sun, Y.J. Li, S.S. Yang, Z.P. Zhang, Phosphorus adsorption in water and immobilization in sediments by lanthanum-modified water treatment sludge hydrochar, J. Environ. Sci. 44 (6) (2023) 3288–3300, https://doi.org/10.13227/j.hjkx.202207114.
[51] J. Zhao, A. Li, H. Wang, Study on the feasibility and stability of drinking water treatment sludge (DWTS)@zeolite to remove phosphorus from constructed wetlands, J. Environ. Chem. Eng. 10 (6) (2022) 108713, https://doi.org/10.1016/j.jece.2022.108713.
[52] D.W. Boukhvalov, V. Paolucci, G. D'Olimpio, C. Cantalini, A. Politano, Chemical reactions on surfaces for applications in catalysis, gas sensing, adsorption-assisted desalination and Li-ion batteries: opportunities and challenges for surface science, Phys. Chem. Chem. Phys. 23 (2021) 7541–7552, https://doi.org/10.1039/d0cp03317k.
[53] G. Fu, Y. Zhao, S. Zhou, C. Chen, Y. Zhong, Y. Xu, Efficient removal of nitrogen and phosphorus in aqueous solutions using modified water treatment residuals–sodium alginate beads, Environ. Sci. Pollut. Res. 28 (2021) 46233–46246, https://doi.org/10.1007/s11356-021-12586-6.
[54] S. Gao, C. Wang, Y. Pei, Comparison of different phosphate species adsorption by ferric and alum water treatment residuals, J. Environ. Sci. (China). 25 (5) (2013) 986–992, https://doi.org/10.1016/s1001-0742(12)60113-2.
[55] R. Rahmati, V. Sidhu, R. Nunez, R. Datta, D. Sarkar, Correlation of phosphorus adsorption with chemical properties of aluminum-based drinking water treatment residuals collected from various parts of the United States, Molecules 27 (21) (2022) 7194, https://doi.org/10.3390/molecules27217194, 7194.
[56] C.M. Lastoskie, A modified horvath-kawazoe method for micropore size analysis, Stud. Surf. Sci. Catal. 128 (2000) 475–484, https://doi.org/10.1016/S0167-2991(00)80053-1.
[57] M.D. Nguyen, et al., Phosphorus adsorption and organic release from dried and thermally treated water treatment sludge, Environ. Res. 234 (2023) 116524, https://doi.org/10.1016/j.envres.2023.116524.
[58] J.L. Syrjanen, K. Michalski, T. Kawate, H. Furukawa, On the molecular nature of large-pore channels, J. Mol. Biol. 443 (2021) 166994, https://doi.org/10.1016/j.jmb.2021.166994.
[59] M.R. Ament, E.D. Roy, Y. Yuan, S.E. Hurley, Phosphorus removal, metals dynamics, and hydraulics in stormwater bioretention systems amended with drinking water treatment residuals, J. Sustain. Water. Built. Environ. 8 (3) (2022) 04022003, https://doi.org/10.1061/jswbay.0000980.
[60] N. Yuan, C. Wang, Y. Pei, Investigation on the eco-toxicity of lake sediments with the addition of drinking water treatment residuals, J. Environ. Sci. (China). 46 (8) (2016) 5–15, https://doi.org/10.1016/j.jes.2015.12.022.
[61] S. Agyin-Birikorang, G.A. O'Connor, Lability of drinking water treatment residuals (WTR) immobilized phosphorus: aging and pH effects, J. Environ. Qual. 36 (4) (2007) 1076–1085, https://doi.org/10.2134/jeq2006.0535.
[62] B. Wu, J. Wan, Y. Zhang, B. Pan, I.M.C. Lo, Selective Phosphate Removal from water and wastewater using sorption: process fundamentals and removal mechanisms, Environ. Sci. Technol. 54 (9) (2019) 50–66, https://doi.org/10.1021/acs.est.9b05569.
[63] S. Gubernat, et al., Removal of phosphorus with the use of marl and travertine and their thermally modified forms—factors affecting the sorption capacity of materials and the kinetics of the sorption process, Materials 16 (3) (2023) 1225, https://doi.org/10.3390/ma16031225.
[64] M. Iqbal, M.A. Hanif, U. Rashid, M.I. Jilani, F.A. Alharthi, E.A. Kazerooni, Optimization and kinetic study of treating dye-contaminated wastewater using bio-composite synthesized from natural waste, Separations 10 (7) (2023) 386, https://doi.org/10.3390/separations10070386, 386.
[65] N. Tolazzi, E. Steffani, E. Barbosa-Coutinho, J.B. Severo Júnior, J.C. Pinto, M. Schwaab, Adsorption equilibrium models: computation of confidence regions of parameter estimates, Chem. Eng. Res. Des. 138 (2018) 144–157, https://doi.org/10.1016/j.cherd.2018.08.027.
[66] S. Karimi, M. Tavakkoli Yaraki, R.R. Karri, A comprehensive review of the adsorption mechanisms and factors influencing the adsorption process from the perspective of bioethanol dehydration, Renew. Sust. Energy Rev 107 (2019) 535–553, https://doi.org/10.1016/j.rser.2019.03.025.
[67] G. Miglioranza, M. Schwaab, Generalization and evaluation of the analytical solution of intraparticle diffusion models in finite batch adsorption, Macromol. React. Eng. 17 (4) (2023) 2300018, https://doi.org/10.1002/mren.202300018.
[68] X. Li, J. Cui, Y. Pei, Granulation of drinking water treatment residuals as applicable media for phosphorus removal, J. Environ. Manage 213 (2018) 36–46, https://doi.org/10.1016/j.jenvman.2018.02.056.
[69] Y. Jiang, T. Deng, K. Yang, H. Wang, Removal performance of phosphate from aqueous solution using a high-capacity sewage sludge-based adsorbent, J. Taiwan Inst. Chem. Eng. 76 (2017) 59–64, https://doi.org/10.1016/j.jtice.2017.04.002.
[70] W.A. Galinada H. Yoshida, Intraparticle diffusion of phosphates in OH-type strongly basic ion exchanger, AIChE J. 50 (11) (2004) 2806–2815, https://doi.org/10.1002/aic.10261.
[71] G. Fu, Y. Zhao, S. Zhou, C. Chen, Y. Zhong, Y. Xu, Efficient removal of nitrogen and phosphorus in aqueous solutions using modified water treatment residuals–sodium alginate beads, Environ. Sci. Pollut. Res. 28 (4) (2021) 1–14, https://doi.org/10.1007/s11356-021-12586-6.
[72] D. Banerjee, D. Das, U. Ghosh, S. Banerjee, B. Das, Study of various methods and technologies used in wastewater treatment to control water pollution. https://link.springer.com/chapter/10.1007/978-981-16-6893-7_2424, 2022. (Accessed 25 March 2024).
[73] S.Y.N. Jiang, et al., Adsorption of phosphorus by modified clay mineral waste material relating to removal of it from aquatic system, Int. J. Environ. Monit. Anal. 2 (1) (2014) 36–44, https://doi.org/10.11648/j.ijema.20140201.14.
[74] M. Tanyol, V. Yonten, V. Demir, Removal of phosphate from aqueous solutions by chemical- and thermal-modified bentonite clay. Water, Air. Soil. Pollut. 226 (8) (2015) 269, https://doi.org/10.1007/s11270-015-2538-8.
[75] P. Xiong, Y. Qiu, Q.C. Wang, Phosphorus removal performance and resource utilization of ceramic adsorbent materials, Environ. Eng. Sci. 41 (5) (2024) 190–203, https://doi.org/10.1089/ees.2023.0334.
[76] S. Hosseinpour, M. Hejazi-Mehrizi, H. Hashemipour, M.H. Farpoor, Adsorptive removal of phosphorus from aqueous solutions using natural and modified coal solid wastes, Water Sci. Technol. 87 (6) (2023) 1376–1392, https://doi.org/10.2166/wst.2023.068.
[77] W. Xiong, J. Tong, Z.Y. Guangming, Zeng, Y. Zhou, D. Wang, P. Song, R. Xu, C. Zhang, M. Cheng, Adsorption of phosphate from aqueous solution using iron-zirconium modified activated carbon nanofiber: performance and mechanism, J. Colloid Interface Sci. 493 (2017) 17–23, https://doi.org/10.1016/j.jcis.2017.01.024.
[78] M.A. Butkus, D. Grasso, C.P. Schulthess, H. Wijnja, Surface complexation modeling of phosphate adsorption by water treatment residual, J. Environ. Qual. 27 (5) (1998) 1055, https://doi.org/10.2134/jeq1998.00472425002700050010x.
[79] S. Smith, I. Takács, S. Murthy, G.T. Daigger, A. Szabó, Phosphate complexation model and its implications for chemical phosphorus removal, Water Environ. Res. 80 (5) (2008) 428–438, https://doi.org/10.1002/J.1554-7531.2008.TB00349.X.
[80] R. Duan, C.B. Fedler, Modeling phosphorus adsorption onto polyaluminium chloride water treatment residuals, Water Supply 21 (1) (2021) 458–469, https://doi.org/10.2166/ws.2020.322.
[81] M.J. Iqbal, B. Zaman, M.A. Budihardjo, Utilization of recycled and waste material in construction - a review, IOP Conf. Ser. Earth Environ. Sci. 1268 (2023) 012046, https://doi.org/10.1088/1755-1315/1268/1/012046.
[82] H.S. Kristensen, M.A. Mosgaard, A. Remmen, Integrating circular principles in environmental management systems, J. Clean. Prod. 286 (2021) 125485, https://doi.org/10.1016/j.jclepro.2020.125485.
[83] T. Kamizela, M. Worwag, Processing of water treatment sludge by bioleaching, Energies 24 (2020) 6539, https://doi.org/10.3390/en13246539.
[84] H. Postila, P. Rossi, E. Heiderscheidt, Coagulant precipitated precipitated and biologically stabilized sewage sludge impacts nutrient availability, and risk of nutrient and micropollutant leaching in sludge-amended soils, EGU Gen. Assem. 23 (2023) EGU23–14857, https://doi.org/10.5194/egusphere-egu23-14857.

[85] L. Tang, M. Gao, S. Liang, S. Wang, X. Wang, Enhanced biological phosphorus removal sustained by aeration-free filamentous microalgal-bacterial granular sludge, Water Res. 253 (2024) 121315, https://doi.org/10.1016/j.watres.2024.121315.
[86] T.F. Alsawy, E. Rashad, M. El-Qelish, R.H. Mohammed, A comprehensive review on the chemical regeneration of biochar adsorbent for sustainable wastewater treatment, npj Clean Water 5 (2022) 29, https://doi.org/10.1038/s41545-022-00172-3.
[87] S.A. Abo-El-Enein, A. Shebl, S.A. Abo El-Dahab, Drinking water treatment sludge as an efficient adsorbent for heavy metals removal, Appl. Clay Sci. 147 (2017) 343–349, https://doi.org/10.1016/j.clay.2017.06.027.
[88] O. Hernandez-Ramirez, A. Thompson, The different approaches to chemical phosphorus removal across the UK wastewater industry, Water Environ. J. 38 (2) 301-307, https://doi.org/10.1111/wej.12909.
[89] B. Clark, E. Apraku, H. Dong, W.A. Tarpeh, Ligand exchange adsorbents for selective phosphate and total ammonia nitrogen recovery from wastewaters, Acc. Mater. Res. 5 (4) (2024) 492–504, https://doi.org/10.1021/accountsmr.3c00290.
[90] R. Dias, M.A. Daam, M. Diniz, R. Mauricio, Drinking water treatment residuals, a low-cost and environmentally friendly adsorbent for the removal of hormones-a review, J. Water Process Eng. 56 (2023) 104322, https://doi.org/10.1016/j.jwpe.2023.104322.
[91] S. Sharma, M.M. Ahammed, Application of modified water treatment residuals in water and wastewater treatment: a review, Heliyon 9 (5) (2023) e15796, https://doi.org/10.1016/j.heliyon.2023.e15796.
[92] X. Zhang, X. Tong, Y. Yang, L. Zhang, X. Zhan, X. Zhang, Behavioral toxicity of TDCPP in marine zooplankton: evidence from feeding and swimming responses, molecular dynamics and metabolomics of rotifers, Sci. Total Environ. 921 (2024) 170864, https://doi.org/10.1016/j.scitotenv.2024.170864.
[93] G. Napolitano, T. Capriello, P. Venditti, G. Fasciolo, A. La, P. Marco, T. Antonella, G. Claudio, A.I. Ferrandino, Aluminum induces a stress response in zebrafish gills by influencing metabolic parameters, morphology, and redox homeostasis, Comp. Biochem. Physiol. C Toxicol. Pharmacol. 271 (2023) 109633, https://doi.org/10.1016/j.cbpc.2023.109633.